Volume 19 | Number 28 | 28 July 2017 | Pages 3859–4034

CrystEngComm

rsc.li/crystengcomm

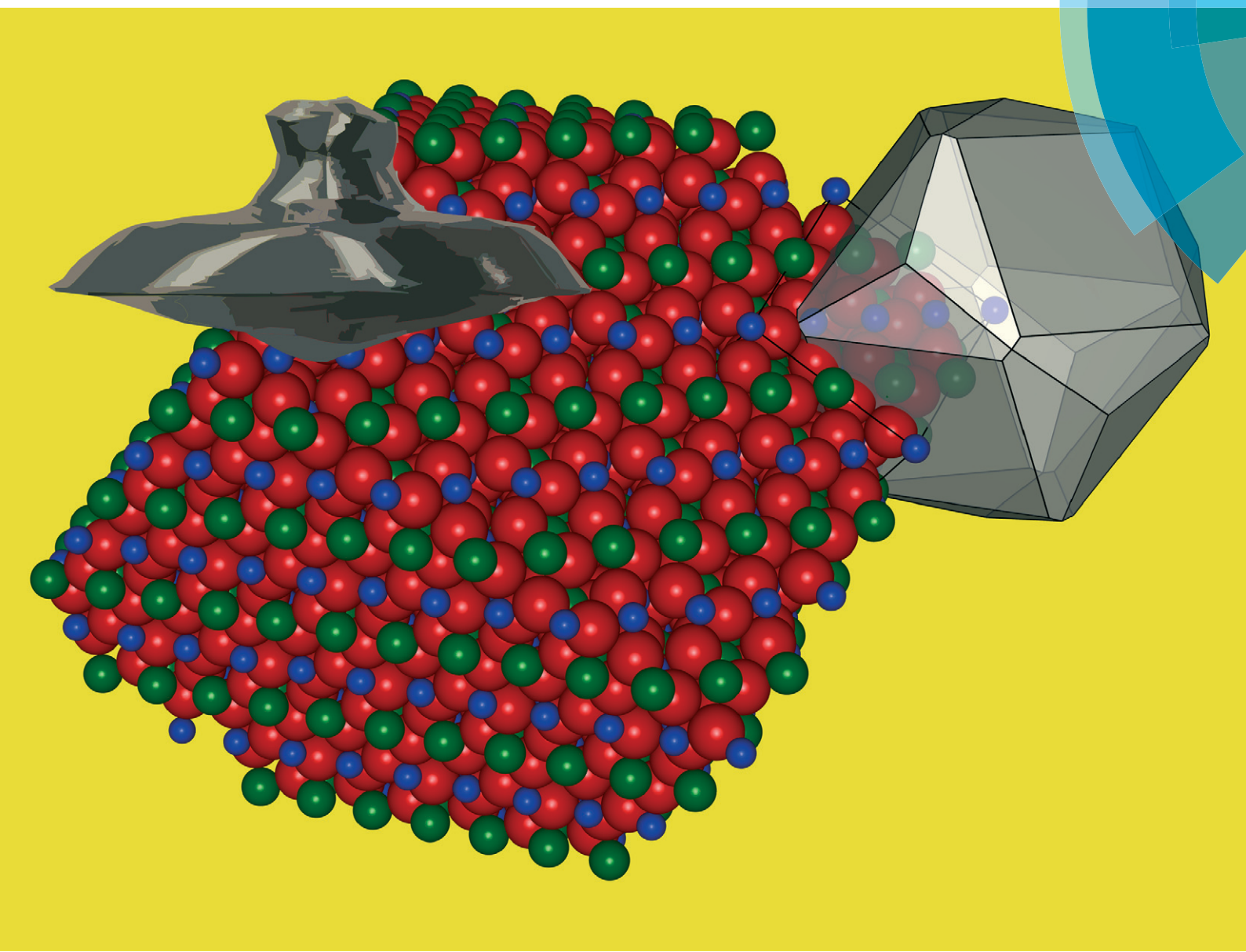

ROYAL SOCIETY OF CHEMISTRY

PAPER

D. Klimm *et al.*

Crystal growth and characterization of the pyrochlore $Tb_2Ti_2O_7$

CrystEngComm

PAPER

View Article Online
View Journal | View Issue

Cite this: *CrystEngComm*, 2017, **19**, 3908

Crystal growth and characterization of the pyrochlore $Tb_2Ti_2O_7$

D. Klimm, *[a] C. Guguschev, [a] D. J. Kok, [a] M. Naumann,[a] L. Ackermann,[b] D. Rytz,[b] M. Peltz,[b] K. Dupré,[b] M. D. Neumann,†[c] A. Kwasniewski,[a] D. G. Schlom [de] and M. Bickermann [a]

Terbium titanate ($Tb_2Ti_2O_7$) is a spin-ice material with remarkable magneto-optical properties. It has a high Verdet constant and is a promising substrate crystal for the epitaxy of quantum materials with the pyrochlore structure. Large single crystals with adequate quality of $Tb_2Ti_2O_7$ or any pyrochlore are not available so far. Here we report the growth of high-quality bulk crystals using the Czochralski method to pull crystals from the melt. Prior work using the automated Czochralski method has suffered from growth instabilities like diameter fluctuation, foot formation and subsequent spiraling shortly after the seeding stage. In this study, the volumes of the crystals were strongly increased to several cubic centimeters by means of manual growth control, leading to crystal diameters of up to 40 mm and crystal lengths of up to 10 mm. Rocking curve measurements revealed full width at half maximum values between 28 and 40″ for 222 reflections. The specific heat capacity c_p was measured between room temperature and 1573 K by dynamic differential scanning calorimetry and shows the typical slow parabolic rise. In contrast, the thermal conductivity $\kappa(T)$ shows a minimum near 700 K and increases at higher temperature T. Optical spectroscopy was performed at room temperature from the ultraviolet to the near infrared region, and additionally in the near infrared region up to 1623 K. The optical transmission properties and the crystal color are interpreted to be influenced by partial oxidation of Tb^{3+} to Tb^{4+}.

Received 17th May 2017,
Accepted 12th June 2017

DOI: 10.1039/c7ce00942a

rsc.li/crystengcomm

1 Introduction

Pyrochlore oxides have the general formula $A_2B_2O_7$ and crystallize in a cubic structure with the space group $Fd\bar{3}m$. They are known for interesting magnetic properties such as giant magnetoresistance.[1] It is generally accepted that the peculiar magnetic properties are related to degeneracy or "frustration" of the ground state of the pyrochlore structure where 3D antiferromagnetic order is impossible, resulting in spin-ice disorder of magnetic moments with nonzero entropy.[2] In addition to frustration of magnetic moments, some pyrochlores show structural disorder of the A- and B-sites. For the pyrochlore $Tb_2Ti_2O_7$, however, it was shown that neither A/B disorder nor oxygen nonstoichiometry plays a significant role, making it an almost ideal, disorder-free pyrochlore model substance,[3] although minor deviations from the ideal Tb/Ti stoichiometry seem to influence the spin–lattice coupling below 1 K.[4] This compound is also considered to be a prospective Faraday isolator, similar to some other complex cubic terbium oxides or halides.[5]

Faraday rotators based on Czochralski (Cz) grown $Tb_2Ti_2O_7$ single crystals were patented recently by some of the current authors.[6] For this prior work, disc-shaped crystals with diameters of 30 mm and several millimeters in length were grown. Crystals with pronounced {111} facets were also reported recently by Guo *et al.*[7] They demonstrated crystals with diameters and lengths of about 20 mm and 16 mm, respectively. In the case of crystals grown by the crucible-free floating zone technique, full width at half maximum (FWHM) values of 1080″ were reported for the 440 reflection using neutron diffraction.[8] These crystals had diameters of 3–5 mm and lengths of up to 20 mm. Until now, no statements on structural quality have been published for Cz grown crystals. In the present work, the growth of bigger single crystals with superior crystal quality is reported for the first time. High crystalline quality is expected to be relevant especially for optical applications requiring low stress birefringence.

[a] *Leibniz-Institut für Kristallzüchtung, Max-Born-Str. 2, 12489 Berlin, Germany. E-mail: detlef.klimm@ikz-berlin.de; Fax: 49 6392 3003; Tel: 49 6392 3018*
[b] *Forschungsinstitut für mineralische und metallische Werkstoffe – Edelsteine/Edelmetalle – GmbH (FEE), Struthstr. 2, 55743 Idar-Oberstein, Germany*
[c] *Leibniz-Institut für Analytische Wissenschaften, Schwarzschildstr. 8, 12489 Berlin, Germany*
[d] *Department of Materials Science and Engineering, Cornell University, Ithaca, NY 14853-1501, USA*
[e] *Kavli Institute at Cornell for Nanoscale Science, Ithaca, NY 14853, USA*
† Current address: Berliner Glas KGaA, Waldkraiburger Str. 5, 12347 Berlin, Germany.

The pyrochlore structure is host to unusual electronic and magnetic properties—including those of spin ice,[2,9] quantum spin ice,[10–16] promising catalysts,[17,18] and possibly Weyl semimetals.[19] This makes it of significant interest as a substrate to enable the growth of high quality thin films with the pyrochlore structure, including pyrochlore heterostructures that are predicted to give rise to odd-parity topological superconductivity.[20] Further, the availability of pyrochlore substrates would enable the strain state in the overlying pyrochlore film to be deliberately tuned to alter its properties. Unfortunately, there are no commercially available pyrochlore single crystal substrates. This has led some to grow epitaxial pyrochlore films on small pyrochlore single crystals grown by the floating-zone method;[21] substrates with higher structural quality, such as those we report, are a prerequisite to the growth of pyrochlore thin films with higher structural quality.

2 Experimental

Stoichiometric melt compositions of $Tb_2Ti_2O_7$ with a melting temperature[22] of about 1860 °C were used for the Cz experiments. As starting materials, dried and mixed powders of Tb_4O_7 and TiO_2 with purities of 99.99% were used. To optimize the crucible filling process, cylindrical bars were made from the powder mixtures by cold isostatic pressing at 200 MPa. The crystal growth experiments were performed using a conventional RF-heated Cz set-up equipped with a crystal balance. Experiments were performed with manual diameter control under a slightly oxygen enriched argon atmosphere (0.155 vol% O_2) at ambient pressure. Iridium crucibles (about 60 mm in diameter and height) embedded in ZrO_2 and Al_2O_3 insulation were used. An actively heated iridium afterheater was placed on top of the crucible. Averaged growth rates were between 2.5 and 30 mm h^{-1}. $Tb_2Ti_2O_7$ single crystals from preliminary experiments with a ⟨111⟩ orientation were used as the seed material.

Rocking curve X-ray diffraction (XRD) measurements were performed on as-grown {111} facets using a high resolution diffractometer (General Electric) with CuKα_1 radiation (λ = 1.5406 Å). $Tb_2Ti_2O_7$ 222 Bragg peaks were used for the evaluation of the crystalline quality. For all scans, the collimated beam had a divergence of 11″ and the measurement spot covered ≈10 mm length of the sample surface. The spot width depended on the primary beam aperture, which was 0.05 mm, 0.3 mm, or 2.0 mm, respectively.

The specific heat capacity, c_p, as a function of temperature T was measured by heat flux differential scanning calorimetry (DSC) with a NETZSCH STA449C. For this purpose, four subsequent heating runs (20 K min^{-1}) from 313 K to 1573 K were performed with one piece of a $Tb_2Ti_2O_7$ crystal in a Pt crucible with a lid in flowing Ar/O_2. $c_p(T)$ was obtained by comparison of these DSC curves with analogous curves that were measured using a sapphire standard sample. The first run showed higher experimental scatter and deviated by up to 5% from the subsequent runs 2–4, probably due to insufficient thermal contact. Therefore, solely the average values of runs 2–4 were used to determine $c_p(T)$.

Measurements of thermal transport were performed with a laser flash apparatus (NETZSCH LFA427). For this purpose, sample slices with 1.34 mm or 1.5 mm thickness were covered with graphite spray on their top and bottom faces. The sample was heated in flowing N_2 to the corresponding temperature step between room temperature and approximately 1380 K, with a typical difference of 50 K between steps. At each step, the bottom side of the sample was irradiated by three shots of a Nd:YAG laser. Measurement of the top side temperature *versus* time resulted in a characteristic line shape that was fitted by Mehling's model[23] for semi-transparent media. This yielded the thermal diffusivity a averaged over the shots. With

$$\kappa = a c_p \rho \quad (1)$$

(ρ = 6.538 g cm^{-3} – mass density[24]), the thermal conductivity was obtained by combining $a(T)$ with the experimental $c_p(T)$. ρ was assumed to be constant, which should result in an uncertainty not exceeding a few percent. Note that there should not be any directional dependence in the thermal conductivity of $Tb_2Ti_2O_7$ because $Tb_2Ti_2O_7$ is cubic and thermal conductivity is a second-rank tensor.[25]

For the room temperature UV/VIS/NIR spectra, two samples were chemo-mechanically polished to about 1 mm thickness. One sample was annealed for 12 h at 1273 K in air in a muffle furnace. Another sample was cut from a crystal grown at the Forschungsinstitut für mineralische und metallische Werkstoffe – Edelsteine/Edelmetalle – GmbH (FEE) and polished to about 1.5 mm thickness. The spectra of the samples were recorded using a Perkin-Elmer Lambda 19 spectrometer and are shown in Fig. 3a. From the measured transmission, Tr, the absorption coefficient was calculated using[26]

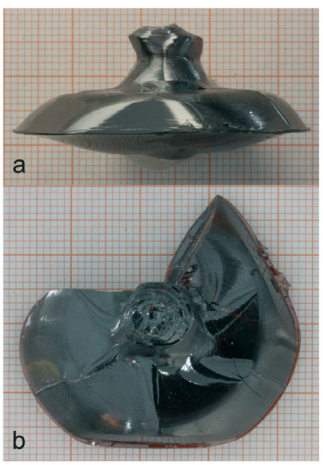

Fig. 1 As-grown $Tb_2Ti_2O_7$ Cz single crystal (length 10 mm, diameter 40 mm) shown from the side (a) and from the top (b), respectively. The crystal was grown at a rate of about 8 mm h^{-1}.

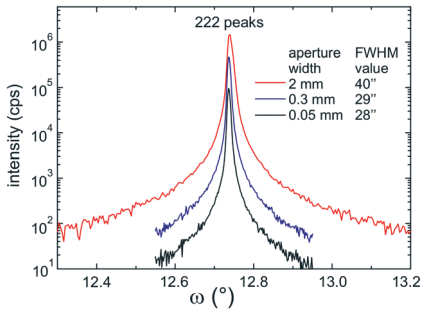

Fig. 2 X-ray rocking curves of 222 peaks measured on an as-grown {111} facet using three different primary beam apertures. The crystal was grown at a rate of about 2.5 mm h^{-1}.

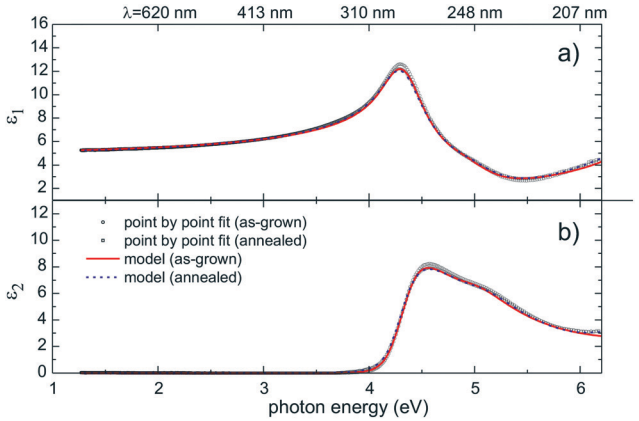

Fig. 4 Comparison of the model and the point-by-point fitted real (a) and imaginary (b) parts of the dielectric functions of the $Tb_2Ti_2O_7$ crystals. The onset of strong absorption around the fundamental band gap is at around 300 nm.

$$\alpha = -\frac{1}{d}\ln\frac{\sqrt{(1-R)^4 + 4\mathrm{Tr}^2R^2} - (1-R)^2}{2\mathrm{Tr}R^2} \quad (2)$$

where d is the sample thickness and R is the reflectivity.

In order to obtain the reflectivity, a Sentech SE850 ellipsometer was used. The ellipsometric parameters Ψ and Δ were recorded at room temperature for angles of incidence between 46° and 74° in steps of 7° over the wavelength range from 200 to 970 nm. By fitting all Ψ and Δ spectra using a three-layer model, which takes into account the surface roughness *via* Bruggeman effective medium approximation,[27] the complex dielectric functions of as-grown as well as annealed $Tb_2Ti_2O_7$ were determined. In the final step, the real and imaginary parts of the dielectric functions obtained by the above procedure were fitted separately for each wavelength without any assumption concerning the line shape, yielding the so-called point-by-point dielectric functions shown in Fig. 4. Details of this procedure were reported elsewhere.[28] The reflectivity was obtained by means of Fresnel coefficients.

High temperature IR spectra were measured for the as-grown and annealed samples in a custom set-up where the samples are mounted in a tube furnace (Hesse Instruments HT-19) that can reach up to 2000 K, giving a maximum possible sample temperature of about 1900 K. The sample compartment can be flushed with different gases. Light from a high power halogen lamp was passed through the sample in the furnace and into an Acton SpectraPro 2300i spectrograph with an InGaAs diode array. The spectrograph was placed far away from the furnace so most of the diffuse thermal radiation was not recorded[29] (the set-up is described in detail in ref. 30). Since the set-up does not have a reference beam, only intensity in arbitrary units is recorded. This is converted to transmission using

$$\mathrm{Tr} = \frac{I(T)}{I(\mathrm{RT})} \times \mathrm{Tr}(\lambda 19) \quad (3)$$

where $I(T)$ is the intensity at temperature T, I(RT) is the room temperature intensity and Tr(λ19) is the transmission measured with the Lambda 19 spectrometer. From these transmission spectra, the absorption coefficients were calculated using eqn (2). The reflectivity was extrapolated to match this wavelength range.

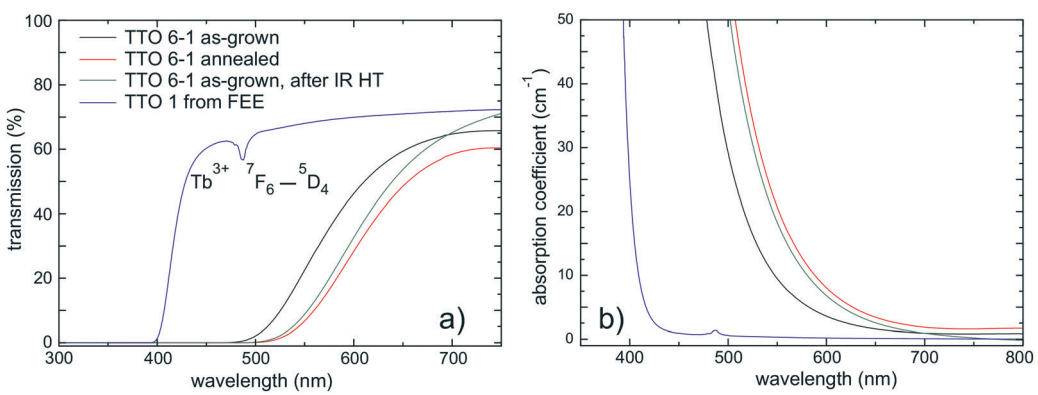

Fig. 3 a) Transmission and b) absorption coefficient spectra of the $Tb_2Ti_2O_7$ crystals. The peak shown by the FEE crystal at about 490 nm is probably the $^7F_6$–$^5D_4$ transition of the Tb^{3+} ions.[33,34] The onset of absorption shifts to longer wavelengths after annealing.

3 Results and discussion

$Tb_2Ti_2O_7$ single crystals with diameters between 30 mm and 42 mm and lengths of up to 10 mm (crystal volumes ≥5.9 cm^3) were grown by the Cz method. Growth instability resulting from low heat flow through the melt/crystal interface could be suppressed substantially by a combination of manual growth control, moderate to high pulling rates and sufficient undercooling of the melt. The most critical part of the growth process was found to be the transition to lateral growth during crystal broadening, which sometimes led to the formation of grain boundaries. If at this stage no grain boundaries were formed, it was unlikely that they were formed later on. The as-grown crystals were transparent in bright light and had brownish to dark-red coloration. Unfortunately, the low thermal conductivity κ (see Fig. 7) made it necessary to use high temperature gradients to maintain sufficient axial heat flux through the growing crystal. Upon cooling to room temperature, this high gradient (directly above the melt surface) usually caused some internal strain. This led to cracking of the crystals into several large parts during handling or sample processing. Cracking could be avoided by cooling the crystals in a lower temperature gradient within the afterheater zone. The crystal in Fig. 1a and b cracked only partially during the last stage of growth, due to contact with metal parts of the growth set-up, most probably due to local foot generation at the crystal rim.

Initially, heterogeneously nucleated boules were grown on Ir tubes, which resulted in multicrystalline growth during the increase of the crystal diameter. Nonetheless, these boules also contained large single crystalline parts suitable for high-quality seed and sample preparation. Single crystals with high structural quality were obtained using ⟨111⟩ oriented seeds and moderate growth rates between 2.5 and about 8 mm h^{-1}. For the single crystalline boules, the structural quality was investigated for a crystal grown at a rate of 2.5 mm h^{-1}. The results of the X-ray rocking curve measurements, performed on an as-grown facet (not polished), show that the FWHM values lie between 28 and 40″ depending on the aperture width of the diffractometer's X-ray source (Fig. 2). Most probably, these slight differences of FWHM values can be explained by a minor surface curvature of the sample or by residual stress, since the crystal was cooled down directly above the melt. The results of the rocking curve measurements show that remarkably high crystal quality can be achieved using the Cz method. This is in contrast to the reported structural quality of $Tb_2Ti_2O_7$ crystals grown under very high thermal gradients using the optical floating zone method.[8]

The structural quality is also higher than for Cz grown $SrTiO_3$ crystals showing similar growth behavior.[31] Potentially, lower thermal gradients resulting from the ≈200 K lower melting temperature here led to higher crystal quality. Additionally, a slightly higher transmissivity in the near infrared region at moderate growth temperatures and presumably a slightly increased thermal conductivity at high temperatures led to higher total heat transport through the crystal and to more stable growth of $Tb_2Ti_2O_7$ than of $SrTiO_3$. Since heat transport is still very low (compared to other oxide crystals like corundum (α-Al_2O_3)), the achievable crystal length with stable growth behavior is limited to 1–2 cm.

Also in contrast to $SrTiO_3$,[32] the infrared absorption of $Tb_2Ti_2O_7$ after annealing in a strongly oxidizing atmosphere

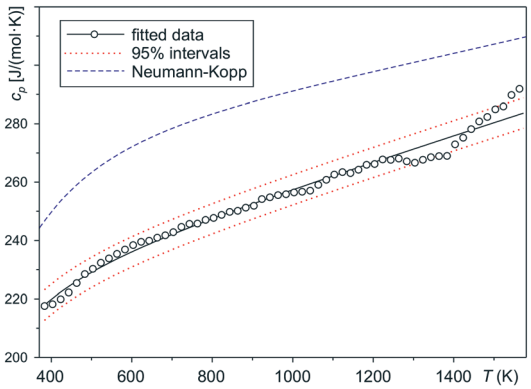

Fig. 6 Measured c_p data, together with a fit to the function in eqn (5) and 95% prediction bands. Also shown for comparison are $c_p(T)$ data calculated according to the Neumann–Kopp rule described by eqn (6) from Tb_2O_3 and TiO_2 data.

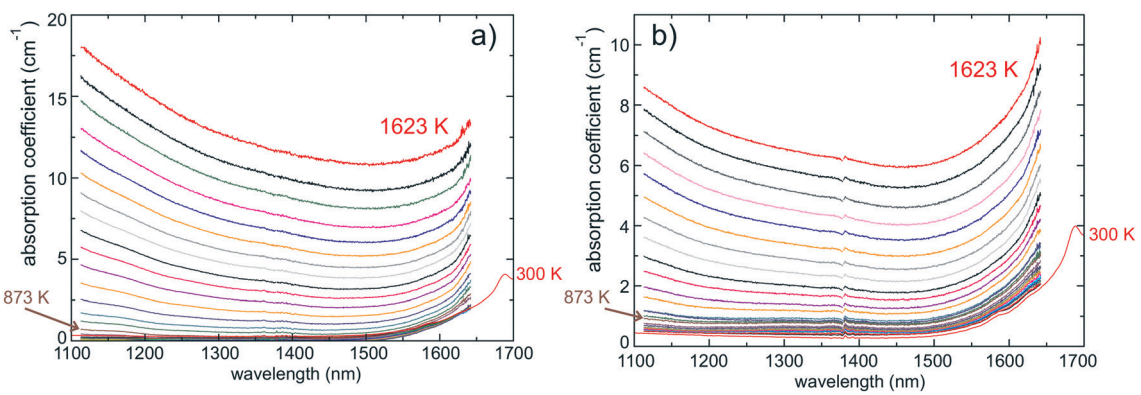

Fig. 5 IR high temperature spectra of a) TTO 6-1 annealed and b) TTO 6-1 as-grown, measured during cooling from 1623 K to RT. The feature near 1380 nm is an artefact.

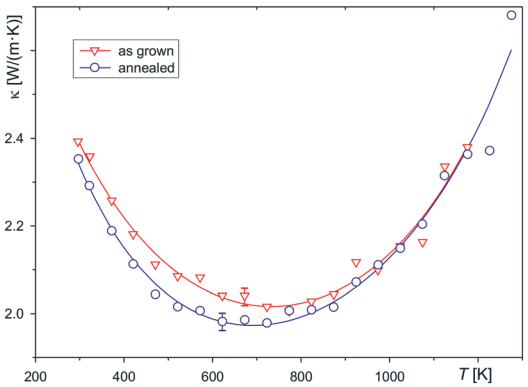

Fig. 7 Thermal conductivity data $\kappa(T)$ of two $Tb_2Ti_2O_7$ samples fitted with the function given in eqn (8). Fit parameters are given in Table 1.

(1273 K in air, p_{O_2} = 212 mbar) is higher than after growth at low oxygen partial pressure (1.6 mbar, see Fig. 5), *i.e.* growth in a highly oxidizing atmosphere is not helpful in stabilizing the growth process. Perhaps there is some potential to increase the lengths of the crystals by application of a very high axial thermal gradient, but this will ultimately lead to lower crystalline quality and cracking of the crystals.

Room temperature transmission spectra of the different $Tb_2Ti_2O_7$ samples are shown in Fig. 3. Remarkably, a sharp absorption edge is observed only for sample TTO 1 grown by some of the current authors (L. A., D. R., M. P., & K. D.) in another Cz set-up, with a lower oxygen partial pressure in the atmosphere (pure nitrogen without oxygen admixture) and from a purer material (99.999% instead of 99.99%) than crystal TTO 6-1. The peak shown by this crystal near 490 nm is the $^7F_6$–$^5D_4$ transition of the Tb^{3+} ions.[33,34] The broad absorption convoluted with the band gap is shifted further to longer wavelengths for the annealed sample.

Thus one can assume that the partial oxidation of Tb^{3+} to Tb^{4+} is responsible for the coloration of the crystals rather than the presence of Ti^{3+}. The stability limits of the different terbium oxides as a function of oxygen fugacity are calculated with FactSage[35] to be

$$TbO_2 \xleftrightarrow{412-582\ K} Tb_6O_{11} \xleftrightarrow{498-685\ K} Tb_7O_{12} \xleftrightarrow{679-963\ K} Tb_2O_3, \quad (4)$$

where the lower temperature represents the stability limit for a virtually oxygen free atmosphere ($\log[p_{O_2}] = -5$), and the higher number is valid in air ($\log[p_{O_2}] = -0.678$). From eqn (4) it is obvious that at least the formation of Tb_7O_{12} = 2 Tb_2O_3 ·3TbO_2 is feasible under all accessible experimental conditions. The stability limit in a virtually oxygen free atmosphere, however, is about 200 K lower compared to air. This raises the chance that Tb_2O_3, and hence pure Tb^{3+}, is frozen in and held metastable also down to room temperature. Tb^{4+} is smaller than Tb^{3+} (90 *vs.* 106.3 pm)[36] but still larger than Ti^{4+} (74.5 pm), and hence Tb/Ti site interchange seems unrealistic, in agreement with recent experimental results.[3] The equilibrium (4) can also explain the higher absorption of air annealed $Tb_2Ti_2O_7$ (Fig. 5) and is in agreement with recent experiments on terbium scandate $TbScO_3$, where a mass gain resulting from partial Tb^{4+} formation was observed upon air annealing.[37] Also $Tb_2Ti_2O_7$ is very dark if grown under high p_{O_2} = 0.4 MPa.[38] It can be calculated that under the given experimental conditions titanium occurs only as Ti^{4+}.[35]

During the high temperature IR measurements, an annealing effect was observed for the as-grown crystal (see Fig. 3), probably due to air leaking into the furnace. Because of that, only the cooling spectra are evaluated. The high temperature spectra of both samples are qualitatively very similar, but the absorption coefficients are much higher for the annealed sample (see Fig. 5). The rise of the absorption coefficient with temperature is fairly monotonic (see Fig. 5), and the shape of the spectra does not match free carrier absorption, which is proportional to λ^2. There is an increase in absorption at the long wavelength edge of the spectra, but this is just the edge of the peak at around 1700 nm which is shown in the room temperature spectra. It appears that less than about 10^{17} cm^{-3} free electrons are present, since this is usually the required approximate concentration for a significant absorption.[26] With rising temperature, the absorption on the low wavelength side increases faster than in other parts of the spectrum (see Fig. 5). This might be caused by the shifting or broadening of the Tb^{4+} absorption that obscures the band gap.

The DSC measurements did not show significant hints of any phase transformations over the experimental range 383 K $\leq T \leq$ 1573 K. Larger deviations from the smooth behavior of $c_p(T)$ at $T >$ 1300 K (Fig. 6) are not reproducible and result from experimental scatter and some drift because at high T the DSC signal is not solely influenced by thermal conduction. The experimental data could be fitted satisfactorily by a simple expression

$$c_p = a + bT + c/T^2 \quad (5)$$

with parameters a = 215.87, b = 0.0436, $c = -2.154574 \times 10^6$, and c_p given in J mol^{-1} K^{-1}. Often the Neumann–Kopp rule gives a good approximation for the $c_p(T)$ functions of complex oxides as the sum of the $c_p(T)$ functions of their constituents. In Fig. 6 the $c_p(T)$ data are fitted to eqn (5) and are compared to the sum of the heat capacities of the constituents following the formation reaction

$$Tb_2O_3 + 2TiO_2 \rightarrow Tb_2Ti_2O_7 \quad (6)$$

that is shown as a dashed line. The disagreement can be attributed to the formation energy of reaction (6), which is neglected by the Neumann–Kopp rule.

Because $Tb_2Ti_2O_7$ is cubic, no anisotropy may occur for the second-rank κ tensor.[25] Hence, $\kappa(T)$ is represented by a single value for every T. The function $\kappa(T)$ was measured for several sample slices, and the results were similar for all of them. Fig. 7 shows the experimental points for two samples.

Table 1 Fit function parameters from eqn (8) for the $\kappa(T)$ functions in Fig. 7

Parameter	As-grown	Annealed
$_A$ (W^{-1} m K)	0.2704	0.2334
$_B$ (W^{-1} m)	6.3300×10^{-4}	8.8523×10^{-4}
$_C$ (W^{-1} m K^{-1})	-4.1922×10^{-7}	-5.4826×10^{-7}
$_D$ (W m^{-1} K^{-2})	7.0879×10^{-5}	3.7419×10^{-4}

Typically near $T > 1200$ K the measurements had to be stopped because the experimental scatter became too large and soon the detector signal of the laser flash apparatus diverged. This instability resulted obviously from damage of the graphite absorption layers, probably by chemical reaction of the Ti^{4+} ions with the strongly reducing graphite.

For many materials, the thermal conductivity drops at high $T \gg T_\Theta$ (T_Θ – Debye temperature) following the $\kappa \propto T^{-1}$ law as a result of phonon scattering (Umklapp process),[39] especially for isolators such as most oxides. Hofmeister[40] found for the laser flash thermal diffusivity of several garnets expressions of the type

$$a = A + BT + CT^2 \quad (7)$$

(A, B, C – constants) to be well suited for fitting the thermal dependence. It should be noted that the low variation of c_p at high T allows similar descriptions for $a(T)$ and $\kappa(T)$. The experimental data in Fig. 7, however, showed a clear rise of κ for large $T > 700$ K, which both models fail to explain.

More recently, Glassbrenner[41] performed thermal conductivity measurements for germanium and silicon up to their melting points, T_f. They showed that for all the temperatures, the major contribution to κ is produced by phonons; however, at sufficiently high $T \approx 700$ or 1000 K, respectively, a significant share of heat is transported by electrons. For the lattice thermal resistance $W = \kappa^{-1}$, a dependence of the type described by eqn (7) was found, where the quadratic term is attributed to 4-phonon processes. For temperatures close to T_f, an almost flat $\kappa(T)$ dependence was measured for Si, and for Ge even an increase of $\kappa(T)$ was observed starting at *ca.* 100 K below T_f. Heat transport by free carriers does not, however, seem realistic in the present case, because the optical measurements showed that the electron density is certainly low (under 10^{17} cm^{-3}). On the other hand, the opacity of dielectric materials typically increases with T, diminishing thermal transport by radiation.[42] This is confirmed by the current laser flash measurements where the detector signal shows that the instantaneous heat transport (by radiation) drops with T. It should be noted that also in the inverse spinel $MgGa_2O_4$, which is another oxide crystal with a low carrier density, κ was found to increase at high $T \approx 1200$ K.[43]

The limited range of experimental points and the higher experimental scatter above the minima in the $\kappa(T)$ functions in Fig. 7 do not allow an accurate determination of the temperature dependence of the process that results in an increasing $\kappa(T)$. Here, a linear behavior was found to describe the experimental data well; hence in the empirical formula

$$\kappa = \frac{1}{A + BT + CT^2} + DT \quad (8)$$

the first term is assumed to describe the thermal transport by phonons ($\propto W^{-1}$), and the second (linear) term describes well an additional high-T term that might be related to heat transport by charge carriers (electrons or holes, respectively).

4 Conclusions

High quality single crystals of $Tb_2Ti_2O_7$ were grown using the Czochralski method. The growth conditions used allowed the growth of disc-shaped single crystals up to 10 mm in length and up to 40 mm in diameter. Unfortunately, slow diameter enlargement and stable long-term growth were not possible due to the poor heat transport through the growing crystal. Cracking of the crystals upon cooling was largely prevented by cooling the crystals with a lower temperature gradient.

The temperature dependence of the thermal conductivity is atypical above 700–900 K, because it shows a minimum value of around 2 W m^{-1} K^{-1} and is slightly larger for lower and higher T. The range of minimum thermal conductivity corresponds to the temperature range where optical transmission starts to drop. Besides these intrinsic properties, optical transmission is altered remarkably if the Tb^{3+} ions in the material are oxidized partially to Tb^{4+}.

Despite the fact that high quality crystals were grown by the Czochralski method, it is rather unlikely that $Tb_2Ti_2O_7$ single crystals can be produced on an automated industrial scale. It seems to be more appropriate to use the edge-defined film-fed growth (EFG) method, which is proven to permit excellent control of the growth processes for a variety of materials *e.g.* for rutile,[44] cerium aluminate,[45] rare-earth orthovanadates,[46] and strontium titanate.[31] For all of these oxides, Czochralski growth was less successful since pronounced growth instabilities occurred. These instability issues were often triggered by poor heat transport (low infrared transmissivity and/or low thermal conductivity) through the growing crystals.

Acknowledgements

The authors are grateful to M. Brützam, E. Thiede, M. Imming-Friedland, and M. Rabe for technical assistance and material preparation. We thank D. Siche for reading the manuscript.

References

1 Y. Shimakawa, Y. Kubo and T. Manako, *Nature*, 1996, **379**, 53–55.
2 S. T. Bramwell and M. J. Gingras, *Science*, 2001, **294**, 1495–1501.
3 S.-W. Han, J. S. Gardner and C. H. Booth, *Phys. Rev. B: Condens. Matter Mater. Phys.*, 2004, **69**, 024416.

4 M. Ruminy, L. Bovo, E. Pomjakushina, M. K. Haas, U. Stuhr, A. Cervellino, R. J. Cava, M. Kenzelmann and T. Fennell, *Phys. Rev. B: Condens. Matter Mater. Phys.*, 2016, **93**, 144407.
5 K. T. Stevens, W. Schlichting, G. Foundos, A. Payne and E. Rogers, *Laser Tech. J.*, 2016, 18–21.
6 L. Ackermann and K. Dupré, Terbiumtitanat zur Verwendung als Faraday-Rotator, DE Patent App. DE201010021203, 2011.
7 F. Guo, Y. Sun, X. Yang, X. Chen, B. Zhao, N. Zhuang and J. Chen, *Opt. Express*, 2016, **24**, 5734–5743.
8 J. Gardner, B. Gaulin and D. Paul, *J. Cryst. Growth*, 1998, **191**, 740–745.
9 A. P. Ramirez, A. Hayashi, R. J. Cava, R. Siddharthan and B. S. Shastry, *Nature*, 1999, **399**, 333–335.
10 I. Mirebeau, A. Apetrei, J. Rodríguez-Carvajal, P. Bonville, A. Forget, D. Colson, V. Glazkov, J. P. Sanchez, O. Isnard and E. Suard, *Phys. Rev. Lett.*, 2005, **94**, 246402.
11 F. Bert, P. Mendels, A. Olariu, N. Blanchard, G. Collin, A. Amato, C. Baines and A. D. Hillier, *Phys. Rev. Lett.*, 2006, **97**, 117203.
12 H. D. Zhou, C. R. Wiebe, J. A. Janik, L. Balicas, Y. J. Yo, Y. Qiu, J. R. D. Copley and J. S. Gardner, *Phys. Rev. Lett.*, 2008, **101**, 227204.
13 K. Kimura, S. Nakatsuji, J.-J. Wen, C. Broholm, M. B. Stone, E. Nishibori and H. Sawa, *Nat. Commun.*, 2013, **4**, 1934.
14 A. J. Princep, D. Prabhakaran, A. T. Boothroyd and D. T. Adroja, *Phys. Rev. B: Condens. Matter Mater. Phys.*, 2013, **88**, 104421.
15 A. Yaouanc, P. Dalmas De Réotier, P. Bonville, J. A. Hodges, V. Glazkov, L. Keller, V. Sikolenko, M. Bartkowiak, A. Amato, C. Baines, P. J. C. King, P. C. M. Gubbens and A. Forget, *Phys. Rev. Lett.*, 2013, **110**, 127207.
16 Y. Tokiwa, J. J. Ishikawa, S. Nakatsuji and P. Gegenwart, *Nat. Mater.*, 2014, **13**, 356–359.
17 T. Mallat and A. Baiker, *Chem. Rev.*, 2004, **104**, 3037–3058.
18 N. K. Beck, B. Steiger, G. G. Scherer and A. Wokaun, *Fuel Cells*, 2006, **6**, 26–30.
19 O. Vafek and A. Vishwanath, *Annu. Rev. Condens. Matter Phys.*, 2014, **5**, 83–112.
20 J.-H. She, C. H. Kim, C. J. Fennie, M. J. Lawler and E.-A. Kim, *Topological Superconductivity in Metal/Quantum-Spin-Ice Heterostructures*, 2016, arXiv:1603.02692.
21 L. Bovo, X. Moya, D. Prabhakaran, Y.-A. Soh, A. Boothroyd, N. Mathur, G. Aeppli and S. Bramwell, *Nat. Commun.*, 2014, 3439.
22 L. G. Shcherbakova, V. B. Glushkova, K. N. Guseva, L. G. Mamsurova, L. V. Sazonova and G. E. Sukhanova, *Izv. Akad. Nauk SSSR, Neorg. Mater.*, 1980, **16**, 1445–1449, in russian.
23 H. Mehling, G. Hautzinger, O. Nilsson, J. Fricke, R. Hofmann and O. Hahn, *Int. J. Thermophys.*, 1998, **19**, 941–949.
24 Y. Luan, *PhD thesis*, University of Tennessee, 2011, p. 117.
25 J. J. Nye, *Physical Properties of Crystals*, Clarendon, Oxford, 1957.
26 D. K. Schroder, *Semiconductor Material and Device Characterization*, Wiley, Hoboken, 3rd edn, 2006, ch. 10.4.1.
27 D. A. G. Bruggeman, *Ann. Phys.*, 1935, **416**, 636–664, in german.
28 M. D. Neumann, N. Esser, J.-M. Chauveau, R. Goldhahn and M. Feneberg, *Appl. Phys. Lett.*, 2016, **108**, 221105.
29 D. Schwabe and A. Polity, *Cryst. Res. Technol.*, 2003, **38**, 868–873.
30 D. Kok, K. Irmscher, M. Naumann, C. Guguschev, Z. Galazka and R. Uecker, *Phys. Status Solidi A*, 2015, **212**, 1880–1887.
31 C. Guguschev, Z. Galazka, D. J. Kok, U. Juda, A. Kwasniewski and R. Uecker, *CrystEngComm*, 2015, **17**, 4662–4668.
32 C. Guguschev, D. Kok, Z. Galazka, D. Klimm, R. Uecker, R. Bertram, M. Naumann, U. Juda, A. Kwasniewski and M. Bickermann, *CrystEngComm*, 2015, **17**, 3224–3234.
33 H. Yoshida, K. Tsubakimoto, Y. Fujimoto, K. Mikami, H. Fujita, N. Miyanaga, H. Nozawa, H. Yagi, T. Yanagitani, Y. Nagata and H. Kinoshita, *Opt. Express*, 2011, **19**, 15181.
34 E. G. Víllora, P. Molina, M. Nakamura, K. Shimamura, T. Hatanaka, A. Funaki and K. Naoe, *Appl. Phys. Lett.*, 2011, **99**, 1–4.
35 www.factsage.com, *FactSage 7.0*, GTT Technologies, Kaiserstr. 100, 52134 Herzogenrath, Germany, 2015.
36 R. D. Shannon, *Acta Crystallogr., Sect. A: Cryst. Phys., Diffr., Theor. Gen. Crystallogr.*, 1976, **32**, 751–767.
37 R. Uecker, B. Velickov, D. Klimm, R. Bertram, M. Bernhagen, M. Rabe, M. Albrecht, R. Fornari and D. G. Schlom, *J. Cryst. Growth*, 2008, **310**, 2649–2658.
38 Q. J. Li, L. M. Xu, C. Fan, F. B. Zhang, Y. Y. Lv, B. Ni, Z. Y. Zhao and X. F. Sun, *J. Cryst. Growth*, 2013, **377**, 96–100.
39 G. A. Slack, *Phys. Rev.*, 1962, **126**, 427–441.
40 A. M. Hofmeister, *Phys. Chem. Miner.*, 2006, **33**, 45–62.
41 C. J. Glassbrenner and G. A. Slack, *Phys. Rev.*, 1964, **134**, 1058–1069.
42 J. R. Aronson, L. H. Bellotti, S. W. Eckroad, A. G. Emslie, R. K. McConnell and P. C. von Thüna, *J. Geophys. Res.*, 1970, **75**, 3443–3456.
43 L. Schwarz, Z. Galazka, T. M. Gesing and D. Klimm, *Cryst. Res. Technol.*, 2015, **50**, 961–966.
44 H. Machida, K. Hoshikawa and T. Fukuda, *J. Cryst. Growth*, 1994, **137**, 516–520.
45 P. Arhipov, S. Tkachenko, I. Gerasymov, O. Sidletskiy, K. Hubenko, S. Vasyukov, N. Shiran, V. Baumer, P. Mateychenko, A. Fedorchenko, Y. Zorenko, Y. Zhydachevskii, K. Lebbou and M. Korjik, *J. Cryst. Growth*, 2015, **430**, 116–121.
46 B. M. Epelbaum, K. Shimamura, K. Inaba, S. Uda, V. V. Kochurikhin, H. Machida, Y. Terada and T. Fukuda, *Cryst. Res. Technol.*, 1999, **34**, 301–309.

